Analysis of single quantum-dot mobility inside 1D nanochannel devices

2011 Nanotechnology 22 275201

(http://iopscience.iop.org/0957-4484/22/27/275201)

Nanotechnology **22** (2011) 275201 (9pp) doi:10.1088/0957-4484/22/27/275201

Analysis of single quantum-dot mobility inside 1D nanochannel devices

H T Hoang[1], I M Segers-Nolten[2], N R Tas[1], J W van Honschoten[1], V Subramaniam[2] and M C Elwenspoek[1,3]

[1] Transducers Science and Technology Group, MESA+ Research Institute for Nanotechnology, University of Twente, PO Box 217, 7500 AE Enschede, The Netherlands
[2] NanoBioPhysics Group, MIRA Institute for Biomedical Technology and Technical Medicine, and MESA+ Institute for Nanotechnology, University of Twente, PO Box 217, 7500 AE Enschede, The Netherlands
[3] Freiburg Institute for Advanced Studies (FRIAS), University of Freiburg, Albertstrasse 19, D-79194 Freiburg, Germany

E-mail: hoanghanhhut@yahoo.com

Received 26 August 2010, in final form 28 March 2011
Published 20 May 2011
Online at stacks.iop.org/Nano/22/275201

Abstract
We visualized individual quantum dots using a combination of a confining nanochannel and an ultra-sensitive microscope system, equipped with a high numerical aperture lens and a highly sensitive camera. The diffusion coefficients of the confined quantum dots were determined from the experimentally recorded trajectories according to the classical diffusion theory for Brownian motion in two dimensions. The calculated diffusion coefficients were three times smaller than those in bulk solution. These observations confirm and extend the results of Eichmann *et al* (2008 *Langmuir* **24** 714–21) to smaller particle diameters and more narrow confinement. A detailed analysis shows that the observed reduction in mobility cannot be explained by conventional hydrodynamic theory.

S Online supplementary data available from stacks.iop.org/Nano/22/275201/mmedia

(Some figures in this article are in colour only in the electronic version)

1. Introduction

Nanochannel devices have been used for single-molecule studies because of their extremely small volume. The confining effect of the nanochannels allows single-molecule studies at relatively high concentration, without requiring immobilization of molecules to keep them in focus. The benefits of nanochannel devices may be exploited for single-molecule applications in many fields such as single-molecule physics, chemistry and biology [1–6]. Single-molecule experiments in nanochannels offer the possibility of exquisite control and manipulation of the sample conditions. These studies reveal information that is otherwise hidden within an ensemble of molecules or can only be addressed by indirect approaches [7–9]. Not only have individual fluorescent molecules been observed and identified, but typical single-molecule characteristics, like blinking and bleaching, have been extensively studied [10]. Functional studies of molecular, interaction and binding studies have been performed [11]. Investigations of physical properties at the single-molecule level, like mobility, provide new insights into the properties of individual molecules in nanometer-scale environments.

In the current paper we address the important issue of the viscosity of confined water by measuring the mobility of fluorescent quantum dots. The viscosity of water in confinement is a long disputed subject since the measurements by Churaev *et al* [12] in quartz micro-capillaries. They found an elevation of the (apparent) viscosity by as much as 40% in 0.04 μm radius capillaries. These results could not be reproduced in nanometer thin films in the surface force apparatus (SFA). A dynamic SFA technique revealed a viscosity of water equal to the bulk viscosity, even in 2 nm thin films and under high salt concentrations sufficient to induce a strong repulsive hydration force between mica surfaces [13]. In recent years, silicon-based nanotechnology offers new routes to study the viscosity of liquids in confinement [14, 15]. The measurement of quantum-dot mobility inside nanochannels is expected to provide relatively direct information on liquid viscosity, through application of the Einstein–Stokes relation.

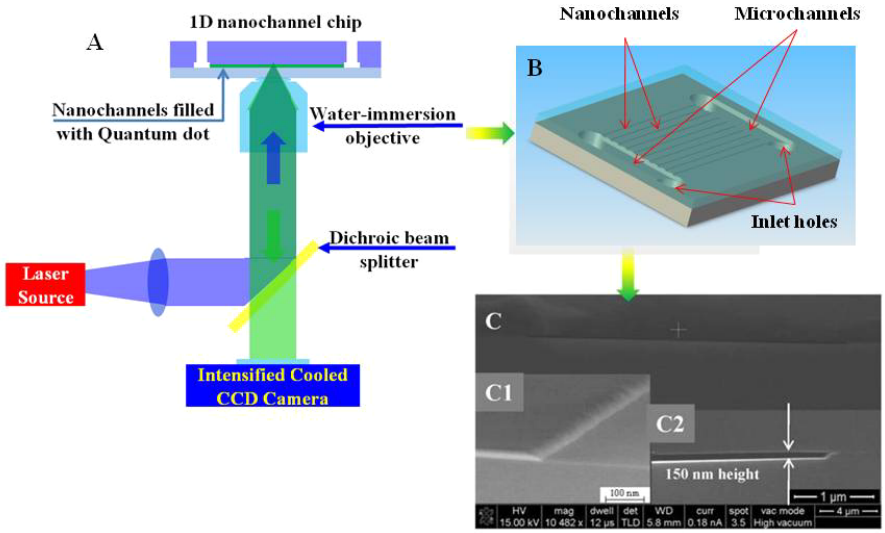

Figure 1. (A) Schematic of the experimental set-up. (B) An artist's drawing of the nanochannel device for the study of single quantum dots. (C) SEM cross section of a 20 μm width nanochannel bonded between a silicon wafer and a thin glass wafer. Inset figure C1: channel wall morphology of the nanochannel formed by wet chemical etching. Inset figure C2: SEM cross section of a 150 nm high nanochannel.

For spheres moving in close proximity parallel to solid surfaces Goldman *et al* [16] modeled the viscous drag, leading to a reduced mobility which deviated from the Einstein–Stokes equation. Banerjee *et al* [17] and Choi *et al* [18] confirmed the theory for nanoparticles (down to 100 nm radius) by tracking their three-dimensional motion using total internal reflection fluorescence microscopy. The lateral mean square displacements (MSD) in the near-wall region were shown to follow the model of Goldman.

In this work, we determine the diffusion coefficients (D) from the Brownian motion of single quantum dots inside 150 nm high nanochannels, visualized by using a high numerical aperture (NA) lens and a sensitive charge-coupled device (CCD) camera. The D values were found to be about three times (60–70%) reduced compared to bulk solution. This is much more than can be explained by the Goldman model. Our result is in qualitative correspondence with the findings of Eichmann [19] who found a 50% reduction of the lateral mobility for 57 nm gold nanoparticles confined between glass surfaces (340 nm separated). Kaji *et al* [20] found a three times lower than expected diffusion coefficient for 50 nm carboxylated polystyrene nanospheres in 400 nm high nanochannels. In the latter case the reduced mobility observed was attributed to an enhanced viscosity of water in nanoconfinement. We will review and analyze in detail different mechanisms that can contribute to the observed decrease in quantum-dot mobility.

2. Experimental details

2.1. Fabrication of 1D nanochannel device by wafer bonding

1D nanochannel devices were fabricated based on the approach of Haneveld *et al* [14, 21]. The process was started on a ⟨110⟩ silicon wafer (Okmetic). A 150 nm thick silicon oxide layer was grown by dry thermal oxidation and its thickness was measured by ellipsometry (Plasmos SD 2002). Next, a standard lithography step was applied to create nanochannel structures of 20 μm width. These structures were transferred to the silicon oxide layer by wet chemical etching in BHF solution. Channel height was controlled by the thickness of the silicon oxide layer and by the time to completely etch this layer. For connection of the nanochannels to the macroworld, microchannels were added which were realized using reactive ion etching. For use on an inverted microscope, inlet/outlet ports were fabricated from the back side of the silicon wafer using deep reactive ion etching at cryogenic temperatures. Finally, the nanochannels were covered by a blank borofloat glass wafer (Mark optics) of 170 μm thickness by direct bonding at 400 °C in order to enable observation on the inverted microscope. Before bonding, both wafers were cleaned in Piranha solution (H_2SO_4:H_2O_2 = 3:1). An artist's drawing of a completely fabricated 1D nanochannel device is shown in figure 1(B), while figure 1(C) shows SEM cross-sectional images of the fabricated channels.

2.2. Materials and microscopy

A quantum-dot (QD) solution (Evitag Fort Orange, type T2-MP, carboxyl, CdSe/ZnS, ~25 nm diameter, emission 600 ± 10 nm (Evident Technologies, New York)) was used for experiments. A 12 μM [22][4] stock solution was diluted in Milli$Q$ water (0.7 μS cm^{-1}) to the required concentration of 12 nM. The diameter of the quantum-dot particles given by the supplier was confirmed to be 25 ± 6 nm using dynamic light scattering. Experiments were carried out on a custom-modified inverted fluorescence microscope (Zeiss, Axiovert)

[4] The concentration of the QD stock solution was 12 μM as determined from absorbance spectroscopy using the Beer–Lambert law [22]: $A = \varepsilon cl$, where A is absorbance of the quantum-dot solution at 580 nm (0.28). ε is the extinction coefficient (223 000 l mol^{-1} cm^{-1} at 580 nm), c is the molar concentration (M) and l is the path length (0.1 cm).

(figure 1(A)) at room temperature (21 ± 1 °C) [23]. For excitation a 488 nm argon laser line was focused into the nanochannels by using a 100×, 1.20 NA, water-immersion objective (Leica Planachromat). Fluorescence emission was detected by an air-cooled, intensified CCD camera (Pentamax, Princeton Instruments). Emission was detected with a 610/75 nm band pass filter and a notch filter was used to remove any residual excitation light. Images of 50 μm × 50 μm (512 pixels × 512 pixels) were recorded by using the WinSpec 32 program (Roper Scientific). A series of 40 sequential images were acquired at a rate of 5 frames per second corresponding to 200 ms exposure time. The nanochannels were filled with the QD solution by capillary forces using a macro inlet hole and a microchannel to couple to the nanochannels. Under the influence of these forces, the solution went through the nanochannels and then quickly stopped when the meniscus reached another microchannel at the distal end of the nanochannels.

2.3. Image analysis

The images recorded by the Winspec program were converted to text-image files by ImageJ software [24]. The text-image files were digitized and redrawn in a user-written Matlab program [25]. Positions of single QDs were manually determined from the Matlab images which were recorded as a set of coordinates $\{x_i, y_i\}$, where the index i indicates the order of an image in a sequence. Two-dimensional movements were recorded during three-dimensional trajectories of single QDs. The confinement of the nanochannels in the vertical direction prevented movement out of the focus of the objective lens.

The precise position of a single QD, defined by the center of the diffraction-limited fluorescence spot, was determined using two-dimensional Gaussian fitting. Trajectories were terminated when the QD disappeared due to bleaching or moved out of the tracking window.

3. Theory on Brownian motion

In 1827, Brown [26] observed that small pollen grains suspended in water exhibit a very animated and irregular state of motion. A satisfactory explanation of the Brownian motion did not appear until 1905, when Einstein [27] showed that macroscopic particles suspended in liquids must perform unceasing motions. The Brownian motion was maintained by collisions with surrounding liquid molecules in the absence of external forces. Based on the Stokes equation, describing the force resisting the motion of a spherical particle in a liquid, Einstein presented the relation between the macroscopic diffusion coefficient and microscopic parameters. The diffusion coefficient D of particles depends on their radius, the temperature and the coefficient of viscosity of the surrounding liquid, and is given by the Einstein–Stokes relation [28]:

$$D = \frac{RT}{N_A}\frac{1}{6\pi\eta r} \tag{1}$$

where R is the gas constant, T—the temperature, N_A—the Avogadro number, η—the viscosity of solvent and r—the radius of the particles.

Einstein inferred from the kinetic theory that an ensemble of small suspended particles had to possess osmotic pressure. If this pressure is distributed in a spatially inhomogeneous way, it gives rise to a compensatory diffusion process. He obtained an expression for the diffusion coefficient, written in the form of a partial differential equation describing the relation between the spatial and temporal change of the probability density function $p(\vec{r}, t)$ of the particles in the solution [28]:

$$\frac{\partial p(\vec{r}, t)}{\partial t} = D\nabla^2 p(\vec{r}, t) \tag{2}$$

where $\vec{r}(x, y)$ or $\vec{r}(x, y, z)$ and $\nabla^2 = \partial_x^2 + \partial_y^2$ or $\nabla^2 = \partial_x^2 + \partial_y^2 + \partial_z^2$ for two or three dimensions, respectively. Equation (2) is Fick's second law, which applies for systems containing many particles. Furthermore, Einstein showed in his theory of Brownian motion that this equation also applies for one particle. Assuming that all the particles are in the same coordinate system, Einstein applied equation (2) to determine the probability distribution of irregularly moving particles. Einstein identified the irregular motion of suspended particles as governed by a stochastic process using the probability function $p(x, y, t)$. By solving equation (2) the probability distribution as a function of time is obtained, which yields for one and two dimensions:

$$p(x, t) = \frac{1}{\sqrt{4\pi Dt}} e^{-x^2/4Dt} \tag{3a}$$

$$p(x, y, t) = \frac{1}{4\pi Dt} e^{-(x^2+y^2)/4Dt}. \tag{3b}$$

From comparing the probability density of particle positions with equation (3), the diffusion coefficient can be determined. Furthermore, we can derive the diffusion coefficient of the Brownian particles from the relation between the MSD and the time t [29]:

$$\langle x^2 \rangle = 2Dt \tag{4a}$$

$$\langle x^2 + y^2 \rangle = 4Dt \tag{4b}$$

where the notation $\langle \cdot \rangle$ represents the mean square displacements, averaged over many particles, or averaged using the probability function in the case of a single particle.

4. Results and discussion

4.1. Visualization of single quantum dots

The fabricated nanochannels were filled with a 12 nM QD solution. Figure 2(A) shows that much fewer QDs were observed than expected based on concentration and volume[5]. Although there is no satisfactory explanation for this phenomenon, ion exclusion [30] has been considered as an effect. The sequences of images (figure 3 and movie 1 in supporting material available at stacks.iop.org/Nano/22/275201/mmedia) identified the presence of individual QDs from the instantaneous appearance and disappearance of fluorescence, a demonstration of the well-known blinking behavior, characteristic for single QDs.

[5] In a nanochannel with volume $v = h \times w \times l = 150 \times 10^{-9} \times 20 \times 10^{-6} \times 50 \times 10^{-6} = 15 \times 10^{-17}$ m^3 filled with a 12 nM concentration solution, there are 1080 QDs to be expected.

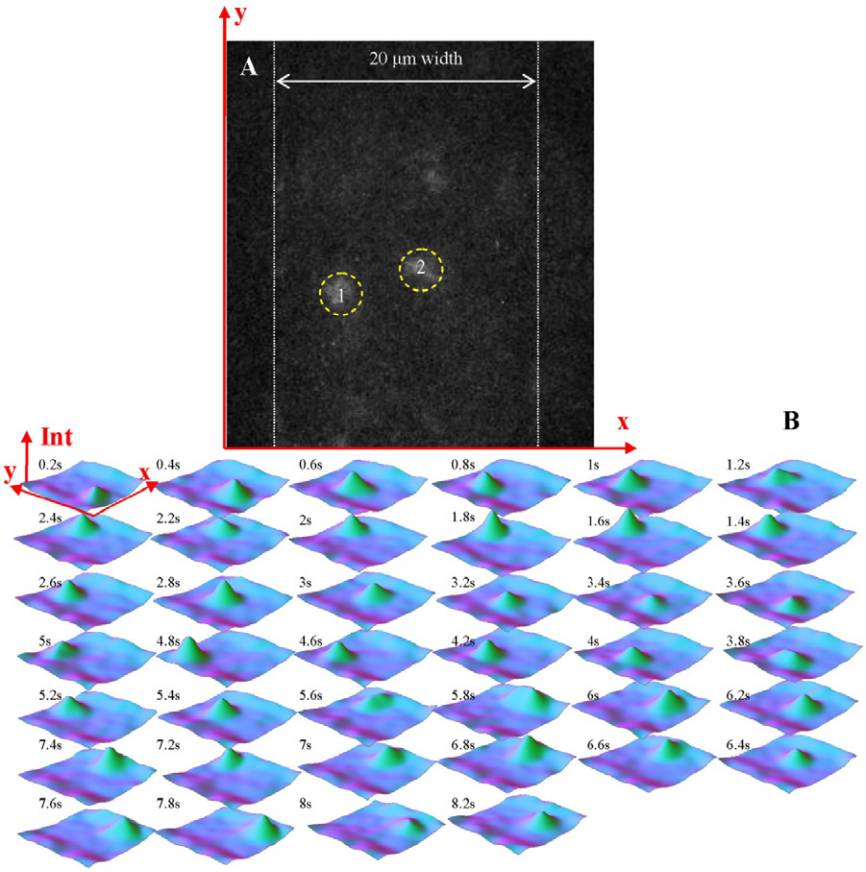

Figure 2. (A) Fluorescence images of single QDs observed in a 150 nm high and 20 μm wide nanochannel; the dotted white lines indicate the channel walls. QDs were marked inside the dashed yellow circles. (B) Surface plots which indicate fluorescence intensity of a single QD performing Brownian motion inside the confined nanochannel (see movie 2 in supporting material available at stacks.iop.org/Nano/22/275201/mmedia).

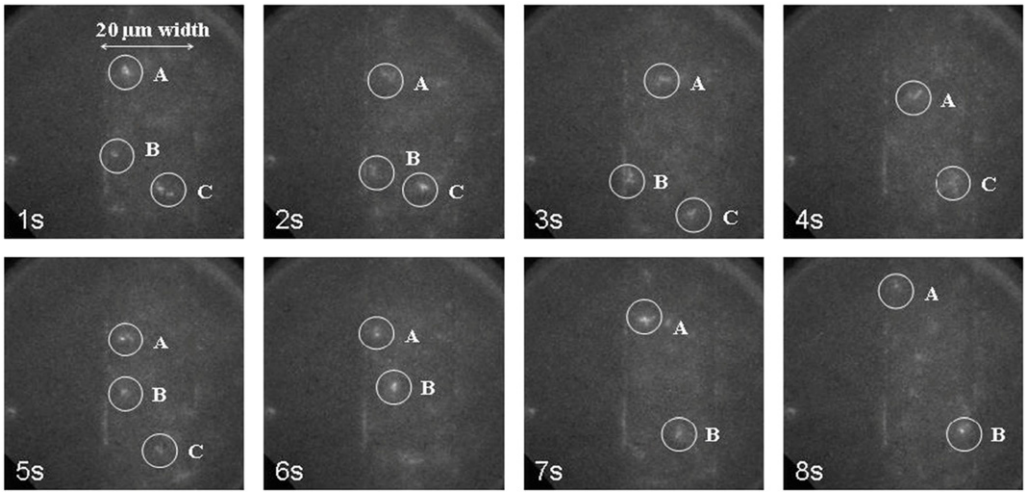

Figure 3. Blinking behavior of individual quantum dots visualized inside 1D nanochannels (150 nm height, 20 μm width). Interfacing of the nanochannels is indicated by the white arrow. In every image of the series, dots could be recognized that were already present in the first image (dots A–C) and could be followed over several consecutive images (2s-, 3s-images); other dots disappeared (dot B in 4s-image) and reappeared (dot B in 5s-image) during imaging. This behavior can be more clearly seen in movie 1 in supporting material (available at stacks.iop.org/Nano/22/275201/mmedia).

4.2. Analysis of quantum-dot mobility

Figure 2(B) shows the fluorescence surface plots of a single QD within 40 sequentially acquired images (movie 2 in supporting material available at stacks.iop.org/Nano/22/275201/mmedia). Analysis of QD mobility was based on two-dimensional projections of three-dimensional trajectories using histograms of displacements with an interval time of $\tau = 200$ ms.

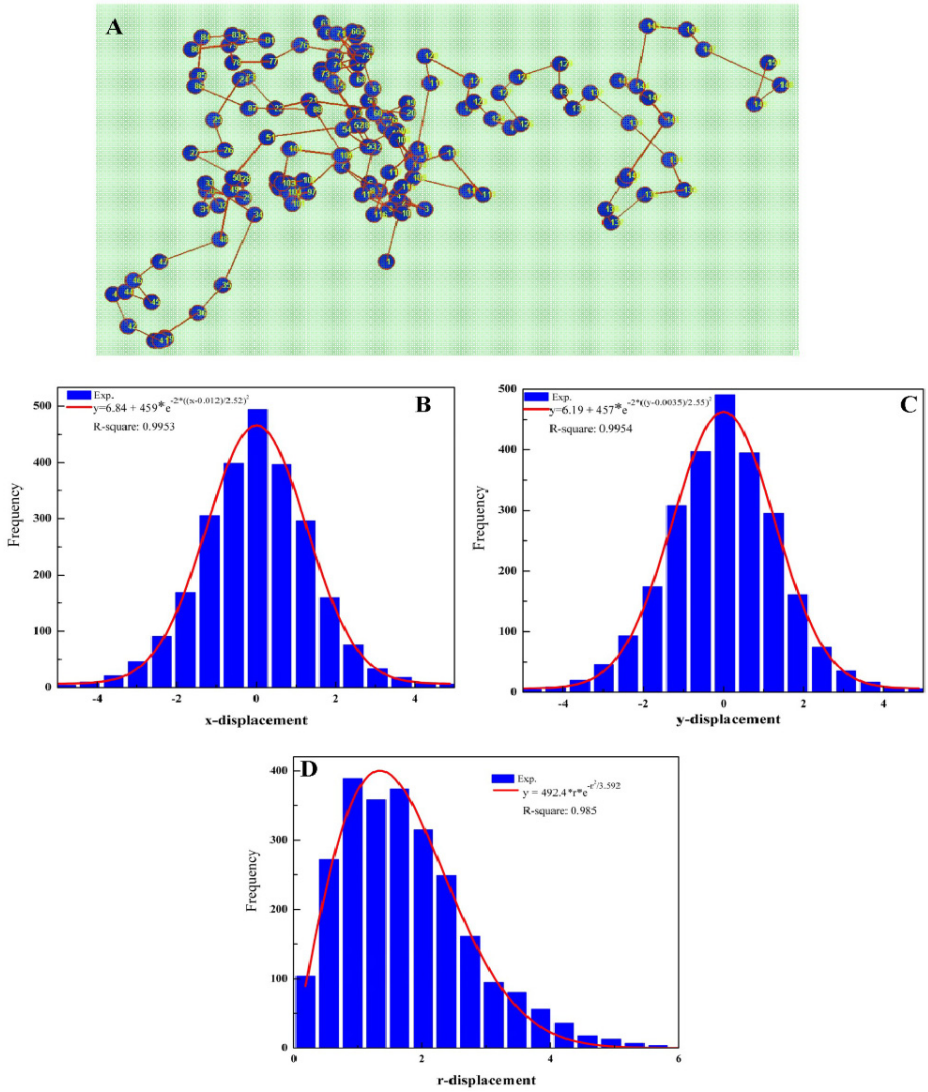

Figure 4. (A) A trajectory of a quantum dot inside a 150 nm high and 20 μm wide nanochannel. (B) and (C) Histograms of x, y displacements of 65 trajectories with 40 steps each in a time lag of 200 ms; x axis is displacements in μm and y axis is frequency; experimental data (bar graphs) are fitted by a Gaussian function indicated by red curves. (D) Histogram of R displacements $R^2 = x^2 + y^2$; experimental data are fitted by a nonlinear least-squares regression function.

Figures 4(B) and (C) show histograms of displacements in the x and y directions (x: across channels, y: along channels). Distributions of x, y displacements satisfied the zero mean.

These experimental data (bar graph) were then fitted by Gaussian distributions (solid lines in figures 4(B) and (C)) [31]. D values were extracted from equation (3*a*) which is the Gaussian function. D_x, D_y values were calculated from the standard deviation σ of the Gaussian distribution, $D_{x,y} = \sigma^2/2\tau$, yielding 5.47 and 5.54 μm^2 s^{-1}, respectively, with $\Re^2 = 0.99$ ($\Re$ is the coefficient of variation). Figure 4(D) presents histograms of R displacements in both dimensions. The experimental data were fitted based on equation (3*b*) by a nonlinear least-squares regression fitting as follows:

$$p^*(R)\,\mathrm{d}R = (R/2Dt)\exp\left(\frac{-R^2}{4\pi Dt}\right)\mathrm{d}R. \qquad (5)$$

The D_R value was extracted to be 4.88 μm^2 s^{-1} with $\Re^2 = 0.98$.

Next, the relation between MSDs ($\langle x^2\rangle$, $\langle y^2\rangle$ and $\langle R^2\rangle$) and time lags was constructed. For a time lag t ($t = m\tau$), MSDs can be determined in two ways: by averaging over all pairs of steps or over independent pairs of steps [32]. In one movie, there are N_s images, separated by an exposure time of 200 ms. Displacements are defined as $R^2(t = m\tau) = (x_{i+m} - x_i)^2 + (y_{i+m} - y_i)^2$. $R(t)$ for defining movements of single QDs in both dimensions is calculated by averaging over all pairs of steps [32] in a time lag t (figure 5):

$$\langle \mathrm{MSD}\rangle = \langle R^2\rangle(t = m\tau) = \frac{1}{N_s - m}\sum_{i=1}^{N_s - m} R_i^2(m\tau). \qquad (6)$$

Figure 6 shows the relation between MSDs and lag times t. The obtained proportional relationship between MSDs and t proved that the Brownian motion of the QDs followed classical diffusion. The diffusion coefficient was calculated from the slope of the straight line fitted to the experimental data.

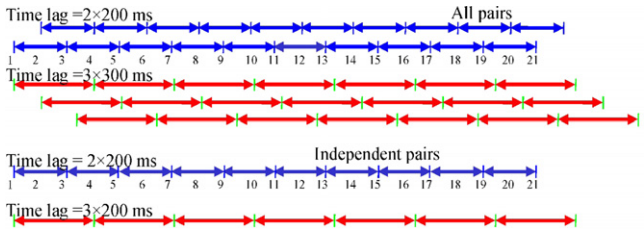

Figure 5. Displacement determination methods for moving positions from 1 to N_s; N_s: number of images in one movie recording the movement of a single quantum dot.

Table 1. D values in $\mu m^2\ s^{-1}$.

	D_x (x displacement)	D_y (y displacement)	D_R (R displacement)
Fitting	5.47	5.54	4.88
MSD	4.94 ± 1.29	5.39 ± 1.29	5.13 ± 1.29

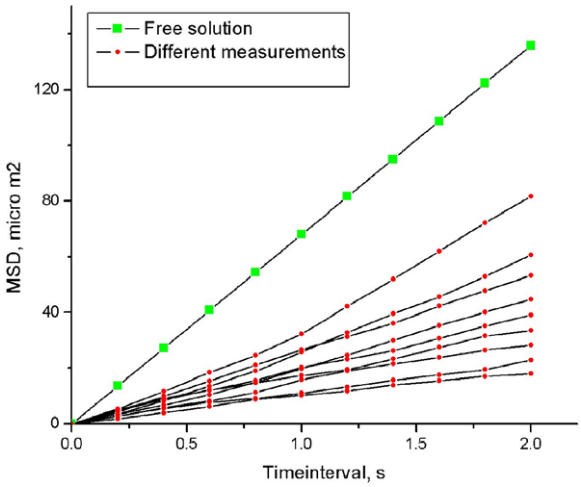

Figure 6. Mean square displacements of the first ten steps of ten trajectories in 150 nm high and 20 μm wide nanochannels.

The distribution of D values calculated from MSD–t curves from 65 different measurements is shown in figure 7. The measured D values (table 1) were about 5–6 $\mu m^2\ s^{-1}$, which is three times smaller than the expected value of 17 $\mu m^2\ s^{-1}$ in bulk solution[6].

4.3. Discussion about observed reduced diffusion coefficient

A reduction of D values in nanochannels compared to bulk solution has been observed in different studies. Lyon *et al* [33] studied the motion of single R6G molecules inside 500 nm diameter capillary channels. Experimental results showed D values which were 50 times lower than in bulk solution. This effect was explained by electrostatic interactions of the charged R6G molecules with the capillary wall. Furthermore, Pappaert *et al* [34] measured the molecular D of fluorescent molecules in nanochannels. The D values for DNA oligomers in 260 nm deep channels were 30% lower than in 2.95 μm channels. Moreover, the reduction of D values inside the nanochannels appeared to correlate with the size of the diffusing molecules, as indicated by a reduction of only 5% for small fluorescein isothiocyanate molecules. Here, the effect was attributed to the presence of the channel walls which increases the number of interactions with the analyte molecules significantly in the case of nanometer-sized channels. In another study, Durand *et al* [35] measured diffusion coefficients of a protein (38 kDa molecular weight) in 50 nm high nanochannels and found D values four orders of magnitude lower than in bulk solution. This was explained by dynamic adsorption and desorption of molecules on glass surfaces.

The slower diffusion coefficients observed inside nanochannels have been attributed to hydrodynamic and electrostatic interactions [33] of the molecules with the channel walls, and to absorption of molecules on the channel walls. More specifically, focusing on nanoparticles of similar sizes as in our study there are a few studies reporting a reduced mobility. Eichmann *et al* [19] captured trajectories of 50 nm gold nanoparticles confined between glass surfaces separated by 350 nm silica colloid spacers. Observed lateral diffusion coefficients as small as 50% of predicted values were explained by hydrodynamic interactions with the confining walls and an electroviscous effect, possibly being intensively enhanced due to overlap of electrostatic double layers around the particles and wall surfaces. Kaji *et al* [20] observed a three times reduced mobility of 50 nm polystyrene beads (carboxylated) in water confined in a 400 nm tall nanochannel. The reduced mobility was explained by an increase of the water viscosity due to confinement.

To explain the deviation of the D values in our experiments with QDs moving in 150 nm high nanochannels, we considered effects such as the modified Stokes drag in confinement and electrostatic interactions. Even though sticking or adsorption of the QDs to the channel walls was considered to contribute to a decrease of D values [33, 34], it was rejected because of the expected repulsion of the QDs from the channel walls since both are negatively charged in our experiments.

From the ratio of the modified Stokes force in confinement and the Stokes force in bulk solution, the expected deviation from the Einstein–Stokes relation can be extracted [16]:

$$\frac{\mu_{\text{confinement}}}{\mu_{\text{bulk}}}\left[1-\frac{9}{16}\left(\frac{r}{d}\right)+\frac{1}{8}\left(\frac{r}{d}\right)^3-\frac{45}{256}\left(\frac{r}{d}\right)^4-\frac{1}{16}\left(\frac{r}{d}\right)^5\right] \tag{7}$$

where μ is mobility of the particle, r—the radius of the particle and d—the average distance from the particles to the channel walls. From equation (7), assuming an average distance $d =$ 65 nm (the distance for the QDs staying at the center plane of the channel), the ratio between the mobility in confinement and in bulk solution appears to be about 0.88, indicating a decrease

[6] From the Einstein–Stokes relation (equation (1)), the diffusion coefficient of the QDs in bulk solution was calculated based on their radii and viscosity of media:

$$D=\frac{RT}{6\pi N_A \eta r}=\frac{8.31\times 298}{6\pi\times 6.023\times 10^{23}\times 0.001\times 12.5\times 10^{-9}}=17\ (\mu m^2\ s^{-1}).$$

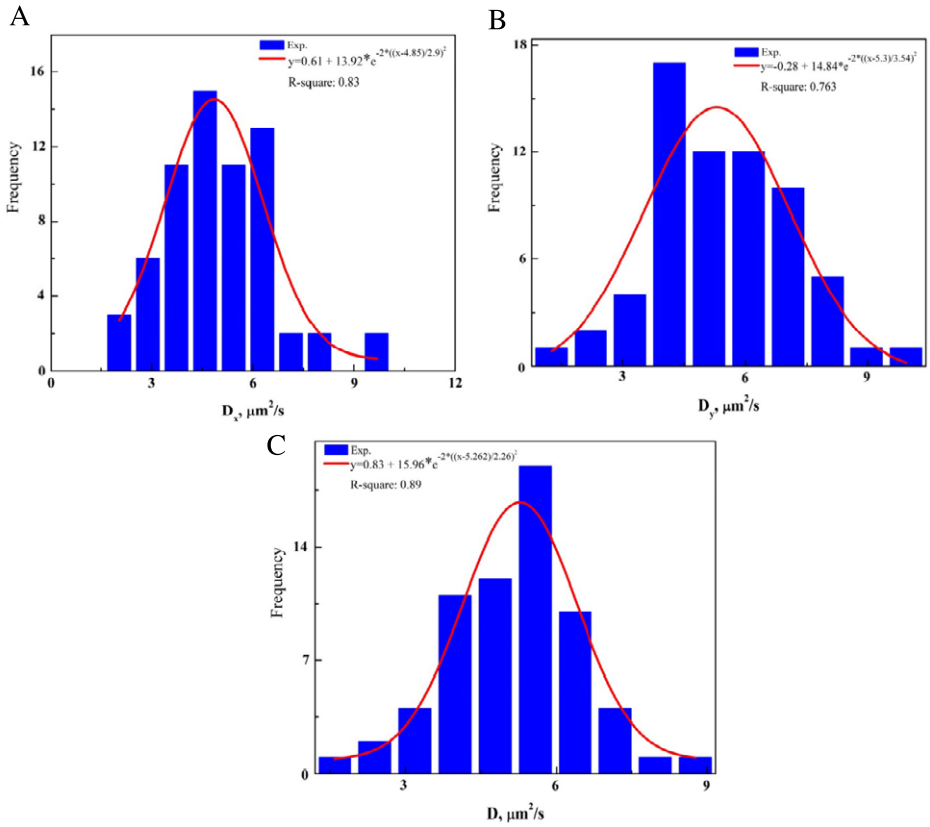

Figure 7. Distribution of D values of QDs in nanochannels (height of 150 nm, width of 20 μm and length of 50 μm, 65 measurements). The bar graphs are experimental data; the red curves are Gaussian fitting functions. Most frequent values are from 5.5 to 6 μm^2 s^{-1}. (A) D_x, (B) D_y and (C) D_R.

of mobility due to hydrodynamic interactions between particles and channel walls. Although the generated reduction is only moderate, we consider hydrodynamic effects as partially responsible for the three times lower mobility observed in our experiments. Note that equation (7) is valid for the ratios d/r ranging from 1 to 10.

Kaji *et al* [20] suggested a change of the bulk viscosity of water due to confinement to be responsible for the reduced mobility. Note that the possible increased viscosity of water near polar or charged walls is a long-disputed subject. Some suggest an increased viscosity that extends of the order of 10 nm into the liquid [12], while other experimental studies indicate that there is no such effect and water retains its bulk viscosity within less than a nanometer distance from the wall [13]. Recent AFM measurements indicate that there is a repulsive structural force and an associated increased viscosity of water which extends about 1 nm into the liquid [15]. This result is consistent with viscosity measurements through analysis of the capillary filling dynamics of nanochannels with a typical diameter of 10 nm [14]. Based on the latter two studies one should conclude that it is unlikely that a real viscosity effect is responsible for the reduced mobility of the QDs confined to a 150 nm tall spacing.

Next, the electroviscous effect was considered. The mechanism is that, when a suspended particle is randomly moving in a quiescent liquid due to thermal motion, surrounding ions in the electrical double layer of this particle are dragged along due to the motion of the other particle. This effect has been described before in the work of Ohshima *et al* [36] and Cox [37] who studied the electroviscous effect on the motion of sedimented particles. Here, the charged particles were sedimented in a liquid without a wall present and the electrical double-layer thickness was very much smaller than the particle size. The ratio between the drag and the ideal Stokes drag is as follows [37]:

$$\frac{\mu_{\mathrm{EVE}}}{\mu_{\mathrm{bulk}}} = 4\left(\frac{(\varepsilon\varepsilon_{\mathrm{o}})^2(kT)^3}{(ze)^4\eta_\infty r^2}\right)\left(G^2+H^2\right) \tag{8}$$

where G and H are defined as [37]

$$G = \ln\tfrac{1}{2}[1+\exp(-\tfrac{1}{2}\tilde{\psi}_p)],$$

$$H = \ln\tfrac{1}{2}[1+\exp(+\tfrac{1}{2}\tilde{\psi}_p)].$$

Here k is the Boltzmann constant, z—the ionic valence, e—the charge of a proton, n_∞—the ionic concentration and $\tilde{\psi}_p$—the dimensionless surface potential of particles. Derivation of equation (8) was based on the assumption that the Debye length, a measure for the electrical double-layer thickness, is smaller than the particle radius. In our experiments however, the Debye length is probably larger than the particle radius and therefore we have to use the numerical calculation presented in figure 1 from Ohshima *et al* [36], resulting in a reduction of D values of about 10%. Note that these models have been

derived for particles in bulk solution. It has been suggested by Eichmann *et al* [19] that, in the presence of a wall and in conditions of double-layer overlap, the reduction of mobility is much greater than predicted by the Ohshima and Cox models. However, so far this hypothesis is not supported by a quantitative model and has not been systematically tested. A logical step to test this hypothesis is to study the dependence of the effect on the electrolyte concentration and zeta potential of the particles. Altogether, we should conclude that at this moment there is no sound theory existing to explain the reduced mobility by us and by other teams.

5. Conclusions

We fabricated nanochannels of 150 nm height that were connected to microchannels and macro inlet ports using a bond-micromachining technique. The nanochannels were used to carry out filling experiments. Visualization of single quantum-dot nanoparticles was realized after filling with a 12 nM solution. The combination of a nanochannel, a high NA lens and a sensitive intensified CCD camera established a platform for single-molecule studies at relatively high concentration. Random movements of single QDs were observed consistent with classical Brownian motion theory. We experimentally determined the diffusion coefficients of single QDs by image analysis revealing the mean square displacements. The diffusion coefficients of single QDs moving inside nanochannels were found to be three times smaller than theoretically expected for 12.5 nm radius particles in bulk solution. The observed reduced mobility confirms and extends the results of Eichmann who found a 50% reduced mobility of 50 nm particles in a 350 nm confinement. The observed reduced mobility cannot be explained by conventional hydrodynamic and electroviscous theories. Follow-up studies should concentrate on modeling of the electroviscous effect under conditions of double-layer overlap, and on experiments in which the dependence of the particle mobility on electrolyte concentration is measured.

Acknowledgments

The authors would like to thank the NanoNed Program (flagship Nanofluidics) for financial support, Dr Nguyen Duy Ha, Leiden University, for fruitful discussion and Dr Marieke Snijder-van As for assistance in fluorescence microscopy.

References

[1] Cosentino C, Amato F, Walczak R, Boiarski A and Ferrari M 2005 Dynamic model of biomolecular diffusion through two-dimensional nanochannels *J. Phys. Chem.* B **109** 7358–64

[2] Wang M, Jing N, Su C B, Kameoka J, Chou C K, Hung M C and Chang K A 2006 Electrospinning of silica nanochannels for single molecule detection *Appl. Phys. Lett.* **88** 033106

[3] Kievsky Y Y, Carey B, Naik S, Mangan N, Ben-Avraham D and Sokolov I 2008 Dynamics of molecular diffusion of rhodamine 6G in silica nanochannels *J. Chem. Phys.* **128** 151102

[4] Douville N, Huh D and Takayama S 2008 DNA linearization through confinement in nanofluidic channels *Anal. Bioanal. Chem.* **391** 2395–409

[5] Stavis S M, Edel J B, Li Y, Samiee K T, Luo D and Craighead H G 2005 Single-molecule mobility and spectral measurements in submicrometer fluidic channels *J. Appl. Phys.* **98** 044903

[6] Pennathur S, Baldessari F, Santiago J G, Kattah M G, Steinman J B and Utz P J 2007 Free-solution oligonucleotide separation in nanoscale channels *Anal. Chem.* **79** 8316–22

[7] Bai C, Wang C, Xie X S and Wolynes P G 1999 Single molecule physics and chemistry *Proc. Natl Acad. Sci. USA* **96** 11075–6

[8] Craighead H 2006 Future lab-on-a-chip technologies for interrogating individual molecules *Nature* **442** 387–93

[9] Ying L 2007 Single molecule biology: coming of age *Mol. BioSyst.* **3** 377–80

[10] Moerner W E 1997 Those blinking single molecules *Science* **277** 1059–60

[11] Baer R and Rabani E 2008 Theory of resonance energy transfer involving nanocrystals: the role of high multipoles *J. Chem. Phys.* **128** 184710

[12] Churaev N V, Soboley V D and Zorin Z M 1971 *Special Discussion on Thin Liquid Films and Boundary Layers* (New York: Academic) pp 213–20

[13] Israelachvili J N 1986 Measurement of the viscosity of liquids in very thin films *J. Colloid Interface Sci.* **110** 263–71

[14] Haneveld J, Tas N R, Brunets N, Jansen H V and Elwenspoek M 2008 Capillary filling of sub-10 nm nanochannels *J. Appl. Phys.* **104** 014309

[15] Li T D, Gao J, Szoszkiewicz R, Landman U and Riedo E 2007 Structured and viscous water in subnanometer gaps *Phys. Rev.* B **75** 115415

[16] Goldman A J, Cox R G and Brenner H 1967 Slow viscous motion of a sphere parallel to a plane wall-I motion through a quiescent fluid *Chem. Eng. Sci.* **22** 637–51

[17] Banerjee A and Kilm K D 2005 Experimental verification of near-wall hindered diffusion for the Brownian motion of nanoparticles using evanescent wave microscopy *Phys. Rev.* E **72** 042101

[18] Choi C K, Margraves C H and Kihm K D 2007 Examination of near-wall hindered Brownian diffusion of nanoparticles: experimental comparison to theories by Brenner (1961) and Goldman *et al* (1967) *Phys. Fluids* **19** 103305

[19] Eichmann S L, Anekal S G and Bevan M A 2008 Electrostatically confined nanoparticle interactions and dynamics *Langmuir* **24** 714–21

[20] Kaji N, Ogawa R, Oki A, Horiike Y, Tokeshi M and Baba Y 2006 Study of water properties in nanospace *Anal. Bioanal. Chem.* **386** 759–64

[21] Hoang H T, Segers-Nolten I M, de Boer M J, Berenschot J W, Tas N R, Haneveld J and Elwenspoek M C 2009 Fabrication and interfacing of nanochannel devices for single-molecule studies *J. Micromech. Microeng.* **19** 065017

[22] Sun J and Goldys E M 2008 Linear absorption and molar extinction coefficients in direct semiconductor quantum dots *J. Phys. Chem.* C **112** 9261–6

[23] Snijder-van As M I, Rieger B, Joosten B, Subramaniam V, Figdor C G and Kanger J S 2009 A hybrid total internal reflection fluorescence and optical tweezers microscope to study cell adhesion and membrane protein dynamics of single living cells *J. Microsc.* **233** 84–92

[24] ImageJ, Image processing and analysis in Java http://rsb.info.nih.gov/ij/

[25] Matlab software from The Mathworks http://www.mathworks.com

[26] Brown R 1828 A brief account of microscopical observations made in the months of June, July and August, 1827, on the particles contained in the pollen of plants; and on the general existence of active molecules in organic and inorganic bodies *Edinburgh New Philoso. J.* **5** 358–71

[27] Einstein A 1905 On the motion-required by the molecular kinetic theory of heat-of small particles suspended in a stationary liquid *Ann. Phys., Lpz.* **17** 549–60
[28] Einstein A 1926 *Investigations on the Theory of the Brownian Movement* ed R Furth (New York: Dover)
[29] Ray D S 1999 Notes on Brownian motion and related phenomena arXiv:physics/9903033v2
[30] Plecis A, Schoch R B and Renaud P 2005 Ionic transport phenomena in nanofluidics: experimental and theoretical study of the exclusion-enrichment effect on a chip *Nano Lett.* **5** 1147–55
[31] Garcia-Palacios J L 2007 Introduction to the theory of stochastic processes and Brownian motion problems arXiv:cond-mat/0701242v1
[32] Saxton M J 1997 Single-particle tracking: the distribution of diffusion coefficients *Biophys. J.* **72** 1744–53
[33] Lyon W A and Nie S 1997 Confinement and detection of single molecules in submicrometer channels *Anal. Chem.* **69** 3400–5
[34] Pappaert K, Biesemans J, Clicq D, Vankrunkelsven S and Desmet G 2005 Measurements of diffusion coefficients in 1D micro- and nanochannels using shear-driven flows *Lab Chip* **5** 1104–10
[35] Durand N F Y, Bertsch A, Todorova M and Renaud P 2007 Direct measurement of effective diffusion coefficients in nanochannels using steady-state dispersion effects *Appl. Phys. Lett.* **91** 203106
[36] Ohshima H, Healy T W and White L R 1984 Sedimentation velocity and potential in a dilute suspension of charged spherical colloidal particles *J. Chem. Soc. Faraday Trans.* 2 **80** 1299–317
[37] Cox R G 1997 Electroviscous forces on a charged particle suspended in a flowing liquid *J. Fluid Mech.* **338** 1–34